HHS Public Access

Author manuscript

ACS Nano. Author manuscript; available in PMC 2023 November 24.

Published in final edited form as:

ACS Nano. 2023 November 14; 17(21): 21093–21104. doi:10.1021/acsnano.3c04420.

Quantitation of Circulating *Mycobacterium tuberculosis* Antigens by Nanopore Biosensing in Children Evaluated for Pulmonary Tuberculosis in South Africa

Xiaoqin Wang[1], **Xiaojun Wei**[1,2], **Marieke M. van der Zalm**[3], **Zehui Zhang**[2], **Nandhini Subramanian**[2], **Anne-Marie Demers**[3,5], **Elisabetta Ghimenton Walters**[3,4], **Anneke Hesseling**[3], **Chang Liu**[1,2,*]

[1]Department of Chemical Engineering, University of South Carolina, Columbia, South Carolina, 29208, USA.

[2]Biomedical Engineering Program, University of South Carolina, Columbia, South Carolina, 29208, USA.

[3]Desmond Tutu TB Centre, Department of Paediatrics and Child Health, Faculty of Medicine and Health Sciences, Stellenbosch University, Cape Town, 8000, South Africa.

[4]Newcastle upon Tyne NHS Hospitals Foundation Trust, Newcastle upon Tyne, NE1 4LP, United Kingdom.

[5]Division of Microbiology, Department of Laboratory Medicine, CHU Sainte-Justine, and Department of Microbiology, Immunology and Infectious Diseases, Faculty of Medicine, University of Montreal, Montreal, Quebec, H3T 1C5, Canada.

Abstract

Nanopore sensing of proteomic biomarkers lacks accuracy due to the ultra-low abundance of targets, a wide variety of interferents in clinical samples, and the mismatch between pore and analyte sizes. By converting antigens to DNA probes via click chemistry and quantifying their characteristic signals, we show a nanopore assay with several amplification mechanisms to achieve attomolar level limit of detection that enables quantitation of circulating *Mycobacterium tuberculosis* (*Mtb*) antigen ESAT-6/CFP-10 complex in human serum. The assay's non-sputum-based feature and low-volume sample requirements make it particularly well-suited for detecting pediatric tuberculosis (TB) disease, where establishing an accurate diagnosis is greatly complicated by the paucibacillary nature of respiratory secretions, nonspecific symptoms, and challenges with sample collection. In the clinical assessment, the assay was applied to analyze

*Address correspondence to: changliu@cec.sc.edu.

ASSOCIATED CONTENT

Supporting Information

Translocation signal trace of unbound CB[6] through an α-HL nanopore (Figure S1); oscillation signal frequencies of DNA probes formed with/without the click reaction and with/without the host-guest interaction (Figure S2); optimization of nanopore assay conditions (Figure S3); representative time-scaled raw current traces of translocations obtained for human serum samples spiked with ESAT-6/CFP-10 antigen at different concentrations (Figure S4); ELISA optimization and test of spiked human serum samples (Figure S5); nanopore assay specificity validation with clinical interferents (Figure S6); 2015 NIH revised classification of intrathoracic tuberculosis case definitions for diagnostic evaluation studies in children (Table S1); comparative analysis of costs for current TB detection techniques (Table S2)

ESAT-6/CFP-10 levels in serum samples collected during baseline investigation for TB in 75 children, aged 0–12 years, enrolled in a diagnostic study conducted in Cape Town, South Africa. This nanopore assay showed superior sensitivity in children with confirmed TB (94.4%) compared to clinical "gold standard" diagnostic technologies (Xpert MTB/RIF 44.4% and *Mtb* culture 72.2%) and filled the diagnostic-gap for children with unconfirmed TB, where these traditional technologies fell short. We envision that, in combination with automated sample processing and portable nanopore devices, this methodology will offer a powerful tool to support the diagnosis of pulmonary TB in children.

Keywords

Nanopore; Pediatric tuberculosis; Blood test; ESAT-6; CFP-10

Utilizing nanometer-scale pores in biological proteins or fabricated from artificial, solid-state membranes, nanopore sensing has shown single-molecule sensitivity and demonstrated excellent accuracy for amino acid identification and nucleic acid sequencing.[1–9] Nanopore sensing has also displayed great potential for protein analysis, and has begun to emerge as a biomarker detection tool for clinical use.[10–15] Theoretically, the concentration of an analyte can be determined by recording and statistically analyzing the frequency of ionic current blockade events induced by translocation of single analyte molecules through the nanopore under an applied electrical potential.[16–20] In practice, to obtain statistically significant numbers of translocation events within a reasonable measurement time, the concentrations of the analyte must be higher than the nanomolar level.[21] Additionally, due to the non-selective translocation of analytes in nanopores and the stochastic nature of the electrical current blockade signals, different analytes often generate similar signals. Therefore, it is difficult to specifically sense ultra-low amounts of biomarkers mixed with a high abundance of interferent molecules in complex clinical specimens, such as serum, using nanopores without any recognition receptors.[14] Existing nanopore technologies are thus primarily used to analyze or sequence high-abundance purified analytes, despite their single-molecule level detection capacity. Furthermore, the electrochemical sensing mechanism and the fixed size of the sensing surface limit the utility of nanopores to only charged macromolecules with sizes comparable to the pore, such as single-stranded DNA (ssDNA).[22, 23]

To realize sensitive and specific detection of low-abundance proteomic biomarkers in human serum by nanopores, we have incorporated click chemistry and host-guest chemistry to develop an assay process that converts proteins to customized ssDNA probes. Taking advantage of the built-in catalytic amplification and specific recognition receptors offered by the ssDNA probes, this nanopore-based testing assay exhibited attomolar (aM) level limit of detection (LOD) when applied to quantify *Mycobacterium tuberculosis* (*Mtb*) specific ESAT-6/CFP-10 antigen complex in human serum samples. Detecting circulating *Mtb* antigens in blood has the potential to improve the diagnosis of tuberculosis (TB) disease and bypass unreliable sputum sampling and consequent sensitivity issues.[24] *Mtb*-derived CFP-10 and ESAT-6 are actively secreted as virulence factors early after infection and also attenuate mycobacterial clearance,[25, 26] implying that their presence in serum may be used to diagnose TB disease.[27–29] However, these antigens circulate at low concentrations

and form antigen complexes that limit detection by standard immunoassays.[30] Our previous studies systematically demonstrated the utility of a mass spectrometry-based blood test that quantifies ESAT-6 and CFP-10 derived peptides, which achieved excellent clinical performance as diagnostic and prognostic biomarkers.[31–34] However, financial and operational barriers of this technology currently hinder its clinical application, as mass spectrometers are rarely affordable in resource-limited regions where TB prevalence is usually the highest. Other blood tests that detect ESAT-6 and CFP-10 TB-specific antigens are the commercial Interferon-gamma release assays (IGRAs), such as are used in the QuantiFERON-TB Gold In-Tube test and the T-SPOT TB test.[35] However, the disadvantages of these commercial IGRAs include the requirement of a large volume of blood, preanalytical sample constraints posed by the need for performing the test on viable bacterial cells, and specialized laboratory infrastructure and expertise. Furthermore, their limited sensitivity in children, particularly in those under five years of age, and inability to discriminate between infection and disease results in high false-positive rates for detecting TB in high-burden settings.[36, 37]

With the recently developed portable nanopore devices,[38, 39] the biosensing assay described herein can directly quantitate circulating ESAT-6/CFP-10 antigen complex and can be incorporated into a point-of-care test device with the necessary accuracy, portability, cost efficiency, and simplicity to fill the diagnostic gaps in high TB-burden areas. Diagnostic performance of this nanopore assay was evaluated by testing clinical samples collected from children enrolled in a prospective TB diagnostic cohort study in Cape Town, South Africa, a high TB-burden setting with an estimated TB incidence of 730 per 100,000 population. The results of the nanopore assay were compared to international consensus clinical case definitions for pulmonary TB in children (described in Methods), using serum samples collected at baseline.[40]

RESULTS

Nanopore Assay for Sensitive and Specific Detection of *Mtb* Antigen Complex

Nanopore sensors operate by monitoring changes to an electrical current as molecules pass through a protein or synthetic nanopore. Traditional signal analysis, which relies solely on dwell time and current blockade of individual signals, often fails to accurately distinguish molecules in complex samples, such as clinical specimens. This is because these parameters are based on the molecular size, weight, or structure of the analytes. In clinical samples, there is a vast number of non-target proteins capable of translocating through or interacting with a given nanopore that may share these physical attributes, leading to erroneous signals with dwell times and current blockades comparable to those of the analyte(s) of interest. As a result, nanopore signals generally demonstrate poor specificity in complex biological fluids like blood.[41–45] The target biomarker of the assay developed in this study is the ESAT-6/CFP-10 heterodimer antigen in blood. Due to its large size, low charge, and low concentration in the complex serum sample, direct detection with a nanopore is challenging and expected to yield marginal accuracy. Therefore, we designed an assay process to immunoprecipitate the antigen complex from serum and convert it to ssDNA probes through a catalytic click reaction to increase the detection sensitivity.

Meanwhile, specificity was greatly improved by utilizing the characteristic signal of a host-guest modification to the probes.[46–48] The assay protocol involved five specific steps (Figure 1a): (1) Enriching ESAT-6/CFP-10 antigen complexes from human serum samples using capture antibody (anti-ESAT-6/CFP-10) modified dynabeads; (2) Forming sandwich structures with detection antibody (anti-ESAT-6/CFP-10) modified copper oxide (CuO) nanoparticles; (3) Releasing Cu^+ by acid treatment; (4) "Clicking" ssDNA-alkyne (DNA-A) with azido adamantane using a Cu^+ catalyst to obtain ssDNA-azido adamantane (DNA-AA); and (5) Generating the host-guest structure of ssDNA probes by adding cucurbit[6]uril hydrate (CB[6]). Translocation of the ssDNA probes through an α-hemolysin (α-HL) nanopore produced highly characteristic signature signals (*i.e.*, oscillation signals) that were clearly distinguished from non-specific signals of DNA-A and DNA-AA (Figure 1b–d). In this nanopore assay, biomarker concentration in the sample is determined only by the frequency of the signals with the oscillation pattern, regardless of their current blockade and dwell time, thus eliminating the associated specificity issue. The oscillation signal frequency correlated with the amount of ssDNA probes and, thus, the concentration of the ESAT-6/CFP-10 antigen complex. No oscillation signals were observed during the translocation of CB[6] in the absence of guest molecules (Figure S1, Supporting Information), confirming that the oscillation pattern can only be induced by the DNA-AA@CB[6] probes, which further establishes the specificity of our nanopore assay. This process engenders a versatile biosensing strategy by combining the nanopore's single-molecule sensitivity to ssDNA with catalytic amplification, resulting in a characteristic signal pattern that allows detection and quantitation with high confidence.[49]

Characterization of ssDNA Probes and Signal Analysis

The ssDNA probe, which generates a characteristic oscillation signal when translocating through an α-HL nanopore, was constructed based on a customized ssDNA backbone with an alkyne-containing thymine base, placed in the middle of a sequence of cytosines. Using a Cu^+ catalyst, released from CuO, a "guest" molecule (azido adamantane) was linked to the alkyne group on the thymine, which could then catch a "host" molecule (CB[6]) in solution to form the host-guest complex (Figure 2a). This structural evolution was confirmed by electrospray ionization mass spectrometry (ESI-MS), showing corresponding peaks of DNA-A (6290.2) and DNA-AA (6467.3) before and after the click reaction (Figure 2b), as well as ^1H nuclear magnetic resonance (NMR) spectra, showing the chemical shift of protons of CB[6] molecules in the host-guest reaction product, DNA-AA@CB[6] (Figure 2c). The characteristic oscillation signals can be induced only by ssDNA probes with the host-guest complex structure. The presence of Cu^+ is necessary for the click reaction and the CB[6] is necessary for the host-guest reaction (Figure S2).

Comparison between corresponding nanopore signals of DNA-A and DNA-AA revealed similar current blockade (I/I_0) and dwell time (Figure 2d and e). The DNA-AA@CB[6] signals showed more signals with higher I/I_0 and longer dwell time than DNA-A and DNA-AA (Figure 2f). Nonetheless, current blockade and dwell time were not used for differentiating DNA-AA@CB[6] signals from the other populations. Upon formation of the DNA-AA@CB[6] host-guest structure, the ssDNA probe showed a characteristic pattern in its nanopore signal, with three consecutive stages, which was used for signal identification

and quantification: Level 1, with long and deep blockades, indicating trapping of the probe in the pore; Level 2, with shorter and smaller blockades, corresponding to ssDNA-AA translocation after dissociation of CB[6]; and Level 3, featuring a transient current fluctuation caused by the oscillation of CB[6] in the pore cavity (Figure 2g).

Assay Optimization and Standard Curves

To increase cost effectiveness, we optimized the assay for the usage of capture and detection antibodies. We selected 2.5 μg per ~5×10^7 dynabeads and 6 μg per 80 μg CuO particles, respectively, for future experiments (Figure S3a and b). To decrease the sampling volume demand for children, we found the lowest serum sample volume needed for each test to achieve the highest sensitivity (100 μL) (Figure S3c). To achieve the shortest sample-to-answer time while maintaining highest reaction efficiency, both click reaction time and host-guest interaction time were optimized to 6 hours (Figure S3d and e). In testing healthy sera spiked with various amounts of ESAT-6/CFP-10 antigen complex, raw current traces indicated a positive correlation between the oscillation signal frequency and the biomarker concentration (Figure 3a). Cumulative counting of oscillation signals in 20-second intervals for each concentration showed steady increases, indicating that recording times between one and four minutes would yield consistent signal frequency, ensuring reliable antigen quantification (Figure 3b). Finally, a standard curve was established between oscillation signal frequency and ESAT-6/CFP-10 antigen complex concentration. The linear range of the curve indicates a limit of quantification (LOQ) of 100 aM and a large dynamic range up to 1 nM (Figure 3c). Further examination of raw data confirmed that oscillation signals could be reliably detected in the 10 aM sample but not in the blank control sample, indicating that the assay achieved 10 aM limit of detection (LOD) (Figure 3c inset and S4). For comparison, an ELISA protocol was developed and optimized. However, its high LOD could not support ESAT-6/CFP-10 detection in clinical samples (Figure S5). Specificity validation was conducted by spiking excessive clinical interferents such as hemolysate, triglycerides, bilirubin, and human albumin into human serum. Individual interferents did not cause significant influence on nanopore test results. However, signal frequency was significantly dampened when the serum sample was contaminated with the combination of all interferents (Figure S6).

ESAT-6/CFP-10 Quantification in Pediatric Samples

To assess the clinical performance of the nanopore assay, pediatric serum samples collected at the Desmond Tutu TB Centre (DTTC, Stellenbosch University, South Africa) were analyzed. Participants (N= 75) were children, 3 months to 12 years old, with presumptive pulmonary TB who were enrolled for further TB evaluation and testing in a diagnostic study. The children were retrospectively categorized into ‘confirmed TB’, ‘unconfirmed TB’, or ‘unlikely TB’ groups, according to the NIH clinical case definitions and consideration of symptomatic responses to treatment (if treated) for TB (Methods, Table 1, and Table S1).[40] After obtaining nanopore test results, the clinical classification was unblinded to the researchers for further analysis. The quantitative nanopore assay results obtained for all children are illustrated in Figure 4a. The mean ESAT-6/CFP-10 level ± the standard deviation (SD) of three experiments for each child is depicted and grouped into one of the three categories (confirmed, unconfirmed, and unlikely TB). The graph shows cases

with exceedingly low (between LOD and LOQ) and undetectable (below LOD) values in magnified insets under the main figure, for clarity. The diagnostic threshold value (1.15 fM) was determined using the receiver operating characteristic (ROC) analysis (Figure 4b) and was used to call if the result was positive (values above the threshold) or negative (values below the threshold) for TB by the nanopore assay. The optimal sensitivity and specificity values provided by the ROC analysis are 94.4% and 81.0%, respectively.

The number of positive (pink blocks) and negative (grey blocks) diagnoses, as defined by the threshold value, determined from the nanopore assay, along with results from the clinical tests (TST, smear, Xpert, and *Mtb* culture) are illustrated in Figure 4c for all children in each group (white blocks indicate children who did not receive a given test). Among the 18 children with confirmed TB, three (participant numbers: P10, P27, and P49, denoted by blue stars) had negative bacteriological results from baseline blood sample; these children were later confirmed for TB by positive Xpert tests performed on follow-up respiratory samples, collected between the first and second months of the study. All confirmed children began antituberculosis treatment at the time of baseline sample collection. The nanopore test results for this group were generally consistent with the results from clinical testing, with the exception of P27, who had ESAT-6/CFP-10 that was quantifiable (above the LOQ), but below the threshold. Notably, this child's chest x-ray (CXR) indicated TB and the child had a positive TST at baseline but was negative on all bacteriological tests (*Mtb* culture, Xpert, and smear).

Of the 36 children with unconfirmed TB, ten were designated as negative by the nanopore assay, with one quantifiable (above the LOQ), but below the threshold. Among these ten, two (P3 and P4, denoted by green stars) should be redesignated as unlikely TB, as discussed in the following section. The remaining 26 children tested positive with above threshold ESAT-6/CFP-10 levels. The TSTs of 11 unconfirmed TB children were positive, eight of which coincided with positives from the nanopore test. None of the unconfirmed TB children tested positive on the smear, Xpert, or culture tests. The remaining 21 children were categorized as unlikely TB; four of these tested positive by the nanopore assay, two of which were deemed false-positives due to the absence of any clinical signs of the disease. It was concluded that the other two children, P21 and P35 (black stars), should be redesignated to the unconfirmed TB group, as discussed further in the following section.

Following NIH definitions, we calculated the nanopore assay's diagnostic sensitivity and specificity within this cohort (Figure 4d). The 94.4% sensitivity for the confirmed TB group was significantly higher than that of the Xpert (44.4%) and *Mtb* culture (72.2%). In the unconfirmed TB group, the nanopore test detected TB in 26 of 36 children, revealing 72.2% of TB-positive children missed by the Xpert and *Mtb* culture methods. It is well-known that the microbiological reference standard is imperfect in children and is likely to miss a proportion of children with TB disease who have low bacillary loads that fall below the detection threshold for both culture and molecular tests.[50–53] Although the 81.0% specificity of the nanopore test fell short of the 100% Xpert and culture specificity, it is creditable considering the test's ability to identify two children initially misassigned to the unlikely TB group (see Discussion), and that TB disease was not ruled out in this group. In terms of overall diagnostic performance, the nanopore test demonstrated enormous potential for the

diagnosis of pediatric TB, outperforming current clinical technologies, including the TST, smear test, and the more sensitive Xpert, and *Mtb* culture.

DISCUSSION

Approximately one million children (<15 years) developed TB in 2019, causing 205,000 TB-related deaths, worldwide.[54] Misdiagnosis can result in undertreatment and ultimately irreversible injury or even death, especially for children with HIV/TB co-infections or disseminated TB. Children with TB frequently have paucibacillary disease, exhibit non-specific symptoms, and are likely to rapidly progress to disseminated TB in the absence of appropriate treatment.[55–58] Less than 15% of children are sputum acid-fast bacilli smear positive, and the "gold standard" *Mtb* culture test yields are only 30%–40%.[58–60] The PCR-based Xpert MTB/RIF sputum assay was introduced in the past decade to improve the speed and specificity of TB testing, but still has poor sensitivity in cases with low bacterial loads, and cannot distinguish between live and nonviable *Mtb*.[61, 62] Moreover, respiratory samples are difficult to obtain from children, especially after symptom improvement, making pediatric TB diagnosis and treatment monitoring even more challenging using sputum-based methods.[55, 61, 62] Immunological tests, such as TST and IGRAs detect the host immune response to *Mtb* infection, but cannot distinguish TB disease from latent TB and are less sensitive in children with immature or compromised immune systems.[63, 64]

Nonspecific symptoms, the paucibacillary nature, and the need for invasive sputum collection all contribute to the difficulty in pediatric TB diagnosis, which may delay antituberculosis treatment initiation.[65] Accurate blood-based assays that use small sample volumes for pediatric TB testing are lacking. Heterodimer ESAT-6/CFP-10 plays a key role in the virulence of *Mtb* infection.[66,26] Diagnostic performance of ESAT-6 and CFP-10 antigens in adult serum and urine samples suggests their considerable promise as biomarkers for a non-sputum-based pediatric TB test.[67–71] We have previously developed a circulating *Mtb* antigen blood assay using mass spectrometry.[31–34] However, its technical and financial barriers significantly impede its clinical applications in resource-limited regions where TB is most prevalent. In this work, we demonstrate a more affordable nanopore assay that enables the quantification of heterodimer ESAT-6/CFP-10 antigens across a wide dynamic range in 100 μL serum samples. A cost analysis of current TB detection techniques has demonstrated that our nanopore sensing system is more cost-effective than several common diagnostic tools for TB screening (Table S2). For real-world application considerations, the acid treatment step, immediately after immunoprecipitation, can eliminate the risk of infection from any pathogens in the blood sample, permitting readout in less controlled environments (*i.e.*, BSL-1 or -2) with safety. Our approach detected TB disease in children within the unconfirmed TB group, missed by current clinical tests (*i.e.,* Xpert and *Mtb* culture). Furthermore, the sensitivity of this test (94.4% in confirmed TB) exceeds the WHO's recommendation (≥66%, which is the average sensitivity of the Xpert MTB/RIF assay) for a non-sputum biomarker test for childhood intrathoracic, microbiologically confirmed TB.[72] Four children (P3, P4, P21, and P35) demonstrated discrepancies between their clinical classification and the results of the nanopore assay, calling for further review of the clinical records of these children (Table 2). Of these, P3 and P4 were classified as unconfirmed TB based on 2015 NIH TB clinical case definitions, with abnormal CXRs indicating lung

cavities and enlarged lymph nodes, respectively, and presenting with well-defined symptoms of pediatric TB disease.[73] However, they tested negative on the TST and were designated as 'symptomatic controls', with no treatment provided and showing no improvement at follow-up appointments. The ESAT-6/CFP-10 levels of these children were undetectable (both with values of fM). Further inspection of their individual clinical analyses revealed that they had received a final alternative diagnosis. Based on this information and the nanopore assays, we conclude that P3 and P4 should be recategorized as unlikely TB. The other two children demonstrating inconsistencies, P21 and P35, were classified as unlikely TB, despite high ESAT-6/CFP-10 levels of 50.59 fM and 49.60 fM, respectively. The CXR of P21 was abnormal, but not suggestive of TB, therefore the child was not initially diagnosed. However, this child started on antituberculosis treatment, four months post-enrollment, due to progressive symptoms and was therefore assigned a treatment status of 'control to case'. This, along with P21's high ESAT-6/CFP-10 level, suggests that our nanopore strategy for testing TB potentially detected an early disease stage in this child. P35 also had an abnormal CXR, displaying consolidation in the lung tissue, but was determined not to be suggestive of TB. Though placed in the unlikely TB group and never treated for TB disease, P35 tested positive on the TST, and was therefore provided with isoniazid preventive therapy; the child showed improvement at follow-up appointments. This could be a case of latent TB, or possibly of incipient/non-severe TB, that was adequately treated with preventive therapy and which our nanopore testing method was able to detect. Based on these analyses, we conclude that P21 and P35 should be categorized as unconfirmed TB. With these recategorizations, the sensitivity of our nanopore assay was calculated at 77.8% in children with unconfirmed TB and 83.3% in children treated for TB disease (confirmed-plus-unconfirmed TB) and the specificity increased from 81.0% to 90.5% (Figure 4d).

To effectively detect ultra-low concentration of ESAT-6/CFP-10 in serum, amplification is crucial for this nanopore sensing platform. There are two amplification mechanisms, incorporated to realize an attomolar level LOD. First, ESAT-6/CFP-10 antigen complexes are immunoprecipitated and formed into sandwich structures with magnetic beads and CuO nanoparticles. An acid treatment then releases Cu^+ to catalyze a click reaction between DNA-alkyne and azido adamantane. This click reaction plays an important role, not only as a signal transducer to transform the ESAT-6/CFP-10 concentration information to DNA probe signal frequency, but also to realize signal amplification. Second, a voltage bias of 160 mV is applied across the nanopore. Under the same applied potential, highly charged DNA probes can translocate the nanopore more efficiently than proteins or peptides, inducing more measurable signals. The ultra-small diameter of the α-HL channel (~1.4 nm) contributes to the high sensing specificity in this platform. The nanochannel only allows one ssDNA molecule to pass at a time, which causes retention of the CB[6] from the host-guest structure of the probe. After separation from the DNA probe, CB[6] oscillates in the pore lumen before translocating or exiting from the entrance. This process induces a characteristic oscillating pattern on the ionic current signal that is not observed for any other molecules in this sensing system and can thus be precisely recorded and quantified to reflect the amount of the target biomarker without false readings.

We also identified limitations of this testing method. First, during the Cu^+-catalyzed click reaction between DNA-alkyne and azido adamantane, an increasing amount of Cu^+

generally increases the amount of product. However, there is a possibility that the amount of product from the reaction may reach a plateau; this, in turn, could dampen the concentration of TB antigen that is detectable in the blood sample. Fortunately, our TB diagnostic method focuses primarily on the low-level existence of ESAT-6/CFP-10 antigens complex; thus, this issue has limited impact on the results of this study. Second, since the biological nanopore inserts into a phospholipid bilayer membrane, the stability of the membrane plays a decisive role in the performance of the pore. Therefore, improvements on techniques that support the stability and durability of the membrane are needed to enhance the efficiency and data validity of the test. Finally, while most standard oscillation signals with Level 1, 2, and 3 can be observed clearly, there are occasionally non-standard oscillation signals that are exceptions. For example, one stage of the translocation process may be indetectable, which is particularly likely for Level 2 due to the brevity of the dissociation process, or analyte may present an oscillation signal that is too short or indistinct. In these cases, manual recognition of the signals is necessary. We believe that through the establishment of machine learning, signal analysis issues can be identified and processed automatically.

CONCLUSIONS

The nanopore-based blood assay for ultrasensitive quantification of circulating *Mtb* antigen ESAT-6/CFP-10 complex demonstrated substantial proficiency in identifying TB in children. Owing to the click chemistry amplification and the nanopore's high sensitivity in detecting DNA, this assay reached attomolar level detection and quantification limits. Direct detection of circulating *Mtb* antigens significantly shortened the sample-to-answer time compared to the "gold standard" *Mtb* culture method for diagnosis, with a turnaround time of approximately two days as opposed to four-eight weeks.[74, 75] Though still longer than the approximately two-hour testing process of the Xpert assay,[76, 77] our nanopore method demonstrated superior sensitivity, reliability, and ease of sample collection. Furthermore, as the nanopore test enables quantitation of ESAT-6/CFP-10 levels, its potential in treatment evaluation through monitoring antigen dynamics warrants continued investigation. Future research objectives include further reducing assay time, technical barriers, and cost by integrating this assay method with portable nanopore readers and microfluidic devices for automated point-of-care testing of TB and other infectious diseases.

METHODS

Participant Recruitment and Categorization

The clinical cohort has been described elsewhere.[78] Children below 13 years of age were recruited from March 2012 to March 2017. Written informed consent from parents/caregivers and ethics approvals from the Stellenbosch University Health Research Ethics Committee and the ethics boards of participating hospitals were obtained. Children living with or without HIV were eligible if they presented with symptoms suggestive of pulmonary TB. Comprehensive TB investigations were completed, including the collection of a minimum of two respiratory samples for *Mtb* bacteriology. Respiratory samples were tested by concentrated smear microscopy for acid-fast bacilli, liquid medium *Mtb* culture (Bactec MGIT 960 system; Becton Dickinson Diagnostic Systems, New Jersey, USA), and Xpert

MTB/RIF assay (Xpert, Cepheid Inc., Sunnyvale, CA). Additional investigations included HIV testing (HIV DNA PCR in children under 18 months of age and HIV enzyme-linked immunosorbent assay (ELISA), for children over 18 months of age), tuberculin skin test (TST; Mantoux, 2 Tuberculin Units PPD RT-23, Statens Serum Institute, Copenhagen), and an antero-posterior plus lateral chest x-ray (CXR), dual read by experts. Whole blood (2 ml) was collected and separated within two hours into serum aliquots by centrifugation as per manufacturer's instructions. All children were then followed for 6 months or until TB treatment completion. International consensus clinical case definitions (NIH definitions) were applied retrospectively at the two-month follow-up to classify participants as having "confirmed TB", "unconfirmed TB", or "unlikely TB". In summary, case definitions were applied as follows: confirmed TB based on microbiologic evidence (*i.e.*, positive *Mtb* culture or positive Xpert results); unconfirmed TB if positive for ≥2 of the following criteria: 1) TB-associated symptoms/signs, 2) abnormal TB-consistent chest radiograph, 3) close TB exposure or immunologic evidence of *Mtb* infection (*i.e.*, with *Mtb* infection, TST positive), or 4) positive response to TB treatment (improvement or resolution of presenting symptoms two months after treatment initiation); unlikely TB if lacked two criteria for unconfirmed TB[40] (Table S1).

Materials and Instruments

Magnetic beads M-270 Carboxylic Acid (30 mg mL^{-1}, 2×10^9 beads mL^{-1}, supplied in purified water) was purchased from Thermo Fisher Scientific (CA, USA). Copper oxide (nanopowder, < 50 nm particle size), bovine serum albumin (BSA), and α-HL from Staphylococcus aureus (lyophilized powder, protein ~60% by Lowry, ≥10,000 units/mg protein) was purchased from MilliporeSigma (Darmstadt, Germany). ESAT-6/CFP-10 rabbit polyclonal antigen complex, and rabbit polyclonal anti-ESAT-6/CFP-10 antibody complex were obtained from MyBioSource (CA, USA). DNA-alkyne was synthesized by Sangon Biotechnology Co. Ltd (Shanghai, China). Micro Bio-Spin P6 gel columns (Tris buffer) were purchased from Bio-Rad (CA, USA). All samples and buffers were prepared in deionized water from a Milli-Q water purification system (Resistivity: 18.2 MΩ/cm, 25 °C, Millipore Corporation). All samples were rotary incubated on Multi-Rotator PTR-35 Grant-bio. All electrophysiology experiments were performed on a Planar Lipid Bilayer Workstation (Warner Instruments). The wash buffer consists of NaCl (0.15 M) and Na_2HPO_4 (10 mM) at pH 7.4. The assay buffer consists of NaCl (0.1 M), Tween 20 (0.025%), BSA (0.1%), and Na_2HPO_4 (10 mM) at pH 7.2. The nanopore work solution consists of KCl (3 M) and Tris (10 mM) at pH 8.0.

Preparation of Capture Antibody-Dynabeads

The dynabeads were washed twice with 2-(N-morpholino) ethane-sulfonic acid (MES, 25 mM, pH 5.0) before use. Both 1-(3-Dimethylaminopropyl)-3-ethyl carbodiimide hydrochloride (EDC) and N-hydroxy succinimide (NHS) were dissolved in cold MES (25 mM, pH 5.0, 1 mL) to reach 50 mg mL^{-1} concentration. Then, EDC solution (50 μL) and NHS solution (50 μL) were added to dynabeads and incubated at room temperature for 30 min for activation. After incubation, the tube was placed on a magnet for supernatant removal. The dynabeads were then washed twice again with MES (25 mM, pH 5.0, 100 μL). Capture antibody (anti-ESAT-6/CFP-10) and MES (25 mM, pH 5.0, 100 μL) were added

to the activated dynabeads and incubated for 2 h at room temperature. After incubation, the tube was again placed on the magnet for supernatant removal. The dynabeads coated with antibodies were incubated with 100 μL Tris (50 mM, pH 7.4) for 30 min to quench the excessive activated carboxylic acid groups and then washed four times with 100 μL phosphate buffer saline (PBS). After blocking with BSA (0.05%, 50 μL), the prepared dynabeads were suspended in PBS (100 μL) and stored at 4°C for further use.

Preparation of Detection Antibody-Copper Oxide Nanoparticles

Copper Oxide Nanoparticles (CuONPs) (1 mg) were added in PBS (1 mL) and were then dispersed by ultra-sonication for 10 min. Detection antibody (anti-ESAT-6/CFP-10) was added to the CuONP solution, drop by drop, for 3 min and incubated for 3 h. Then, the solution was centrifuged at 9000 g for 10 min to remove excess detection antibodies and suspended. The detection antibody-CuONPs was dispersed in PBS (1.5 mL) and centrifuged again (5000 rpm for 10 min) to collect CuONP precipitate. Finally, 10% BSA in PBS (200 μL) was added to the detection antibody-CuONPs and vortexed for 30 min before storage at 4°C.

Formation of Sandwich Structure Compound using Standard and Clinical Samples

Capture antibody-dynabeads (50 μL) were washed with assay buffer (500 μL) five times. To prepare standard samples for calibration curves, assay buffer (400 μL) was added to sterile filtered human serum (100 μL), spiked with various concentrations of ESAT6/CFP-10 antigen and incubated with capture antibody-dynabeads at room temperature for 1 h. After incubation, dynabeads were washed with assay buffer (500 μL) five times, and detection antibody-CuONPs (16 μL) was added and incubated for 1 h. Then the mixture was washed with wash buffer (500 μL) five times to remove the unbound CuONPs. HCl (10 mM, 200 μL) was added and incubated for 10 min to release the Cu^{+}. The solution was adjusted to pH 7.4 and lyophilized. The residue was dissolved in deionized water (20 μL) for ligating DNA probes. A similar protocol was followed for processing clinical serum samples (100 μL). All procedures involving human samples were conducted in a biosafety cabinet located in a Biosafety Level 2 (BSL-2) laboratory. The rest of the assay protocols, after acid treatment, were conducted outside of the biosafety cabinet.

Synthesis of DNA Probes and Characterization

DNA (5′-CCCCCCCCCCTCCCCCCCCCC) modified with an alkyne moiety on the T base (DNA-A, 100 μM, 2 μL), azido adamantane (dissolved in acetonitrile, 200 mM, 2 μL), sodium ascorbate (20 mM, 2 μL), and Cu^{+} solution (obtained as described above, 2 μL) were added to HEPES buffer (100 mM, 2 μL). The reaction was incubated for 6 h at room temperature and then stopped by the addition of EDTA (100 mM, 2 μL) to the reaction. The product was filtered by Micro Bio-spin P6 columns and DNA-AA was obtained. DNA-A and DNA-AA were subjected to mass spectrometry (MS) to confirm their transformation by this click reaction. Then, CB[6] aqueous solution (5 mM, 10 μL) was added to DNA-AA and incubated for 6 h to obtain the final DNA-AA@CB[6]. CB[6] and DNA-AA@CB[6] were subjected to nuclear magnetic resonance (NMR) to ensure the host-guest reaction happened successfully. Finally, the DNA probes were tested as they translocated the α-HL nanopore

by recording the resulting current signals and quantifying the original concentrations of ESAT-6/CFP-10 antigen complex in samples.

Nanopore Sensing and Data Analysis

1,2-Diphytanoyl-sn-glycerol-3-phosphocholine (DPhPC) was used to form a synthetic lipid bilayer membrane across an aperture, 200 μm in diameter, in a 25 μm thick polytetrafluoroethylene film, which divided a fluid chamber into two compartments, *cis* and *trans*. Both compartments contained 1 mL of work solution (3 M KCl, 10 mM Tris, pH 8.0). Each sample was added into the *cis* compartment, which was connected to the ground. A 160 mV potential was applied to the *trans* compartment, which was connected to the head-stage of the amplifier. Ionic currents were measured by using Ag/AgCl electrodes with a patch-clamp amplifier (Warner Instruments, CA, USA). All experiments were carried out at room temperature. Current records were analyzed with Clampfit 10.7 software (Warner Instruments). Characteristic current signature events were manually counted for statistical analysis.

Interference Study

To evaluate the specificity of this assay, typical interferents in human samples, including hemolysate, triglycerides, bilirubin, and human albumin were analyzed. These interferents provided with the kit (INT-01 Routine Interferents, ASSURANCE Interference Test Kit, Sun Diagnostics) were used to obtain diluted experimental concentrations for these studies. Standard human serum sample aliquots (ESAT-6/CFP-10 antigen complex concentration: 100 fM) were spiked with concentrations of hemolysate (5 mg/mL), triglycerides (4.5 mg/mL), bilirubin (80 μg/mL), and human albumin (5mg/mL), individually and simultaneously. These samples were tested by the nanopore assay and compared to a non-interferents sample to estimate their effects on the assay quantification performance.

Supplementary Material

Refer to Web version on PubMed Central for supplementary material.

ACKNOWLEDGMENT

CL acknowledges support from: the National Institute of Allergy and Infectious Diseases (NIAID) awards K22AI136686 and R61AI174295, and the National Science Foundation (NSF) CAREER Award 2047503. MMVDZ is supported by a career development grant from the EDCTP2 program supported by the European Union (TMA2019SFP-2836 TB lung-FACT2), the Fogarty International Centre of the National Institutes of Health (NIH) under Award Number K43TW011028 and the South African Medical Research Council with a SIR grant. EGW was supported by a scholarship for doctoral studies from the Medical Research Council (MRC) of South Africa under the MRC Clinician Researcher Programme, the Faculty of Medicine and Health Sciences at Stellenbosch University (Early Career Grant and Temporary Research Assistantship grant), the Harry Crossley Foundation, and the South African National Research Foundation (Thuthuka programme funding for doctoral students). The characterization work in this study was supported by NSF-MRI Award 1828059 for the acquisition of a Thermo Q-Exactive mass spectrometer. The authors are grateful to the study participants and the medical professionals at Tygerberg hospital, South Africa.

REFERENCES

(1). Clarke J; Wu H-C; Jayasinghe L; Patel A; Reid S; Bayley H Continuous base identification for single-molecule nanopore DNA sequencing. Nature nanotechnology 2009, 4 (4), 265–270.

(2). Schneider GF; Dekker C DNA sequencing with nanopores. Nature biotechnology 2012, 30 (4), 326–328.

(3). Laszlo AH; Derrington IM; Ross BC; Brinkerhoff H; Adey A; Nova IC; Craig JM; Langford KW; Samson JM; Daza R Decoding long nanopore sequencing reads of natural DNA. Nature biotechnology 2014, 32 (8), 829–833.

(4). Workman RE; Tang AD; Tang PS; Jain M; Tyson JR; Razaghi R; Zuzarte PC; Gilpatrick T; Payne A; Quick J Nanopore native RNA sequencing of a human poly (A) transcriptome. Nature methods 2019, 16 (12), 1297–1305. [PubMed: 31740818]

(5). Ayub M; Hardwick SW; Luisi BF; Bayley H Nanopore-based identification of individual nucleotides for direct RNA sequencing. Nano letters 2013, 13 (12), 6144–6150. [PubMed: 24171554]

(6). Soneson C; Yao Y; Bratus-Neuenschwander A; Patrignani A; Robinson MD; Hussain S A comprehensive examination of Nanopore native RNA sequencing for characterization of complex transcriptomes. Nature communications 2019, 10 (1), 1–14.

(7). Howorka S; Siwy ZS Reading amino acids in a nanopore. Nature biotechnology 2020, 38 (2), 159–160.

(8). Wei X; Ma D; Jing L; Wang LY; Wang X; Zhang Z; Lenhart BJ; Yin Y; Wang Q; Liu C Enabling nanopore technology for sensing individual amino acids by a derivatization strategy. Journal of Materials Chemistry B 2020, 8 (31), 6792–6797. [PubMed: 32495805]

(9). Wei X; Ma D; Zhang Z; Wang LY; Gray JL; Zhang L; Zhu T; Wang X; Lenhart BJ; Yin Y N-terminal derivatization-assisted identification of individual amino acids using a biological nanopore sensor. ACS sensors 2020, 5 (6), 1707–1716. [PubMed: 32403927]

(10). Lin Y; Ying Y-L; Shi X; Liu S-C; Long Y-T Direct sensing of cancer biomarkers in clinical samples with a designed nanopore. Chemical Communications 2017, 53 (84), 11564–11567. [PubMed: 28990601]

(11). Guo B; Song P; Zhou K; Liu L; Wu H-C Simultaneous sensing of multiple Cancer biomarkers by a single DNA Nanoprobe in a Nanopore. Analytical Chemistry 2020, 92 (13), 9405–9411. [PubMed: 32539349]

(12). Huang G; Willems K; Soskine M; Wloka C; Maglia G Electro-osmotic capture and ionic discrimination of peptide and protein biomarkers with FraC nanopores. Nature communications 2017, 8 (1), 1–11.

(13). Zhang Z; Wang X; Wei X; Zheng SW; Lenhart BJ; Xu P; Li J; Pan J; Albrecht H; Liu C Multiplex quantitative detection of SARS-CoV-2 specific IgG and IgM antibodies based on DNA-assisted nanopore sensing. Biosensors and Bioelectronics 2021, 181, 113134. [PubMed: 33761415]

(14). Zheng W; Saliba JG; Wei X; Shu Q; Pierson LM; Mao L; Liu C; Lyon CJ; Li C-Z; Wimley WC Nanopore-based disease diagnosis using pathogen-derived tryptic peptides from serum. Nano Today 2022, 45, 101515. [PubMed: 37034182]

(15). Subramanian N; Watson B; Li C-Z; Moss M; Liu C Patterning Amyloid-β Aggregation under the Effect of Acetylcholinesterase using a Biological Nanopore-an in vitro Study. Sensors and Actuators Reports 2023, 100170. [PubMed: 37663321]

(16). Wang G; Zhao Q; Kang X; Guan X Probing mercury (II)–DNA interactions by nanopore stochastic sensing. The Journal of Physical Chemistry B 2013, 117 (17), 4763–4769. [PubMed: 23565989]

(17). Lenhart B; Wei X; Watson B; Wang X; Zhang Z; Li C.-z.; Moss M; Liu C In vitro biosensing of β-Amyloid peptide aggregation dynamics using a biological nanopore. Sensors and Actuators B: Chemical 2021, 338, 129863. [PubMed: 33927481]

(18). Wang Y; Guan X; Zhang S; Liu Y; Wang S; Fan P; Du X; Yan S; Zhang P; Chen H-Y Structural-profiling of low molecular weight RNAs by nanopore trapping/translocation using Mycobacterium smegmatis porin A. Nature communications 2021, 12 (1), 1–14.

(19). Freedman KJ; Otto LM; Ivanov AP; Barik A; Oh S-H; Edel JB Nanopore sensing at ultra-low concentrations using single-molecule dielectrophoretic trapping. Nature communications 2016, 7 (1), 1–9.

(20). Wang X; Stevens KC; Ting JM; Marras AE; Rezvan G; Wei X; Taheri-Qazvini N; Tirrell MV; Liu C Translocation Behaviors of Synthetic Polyelectrolytes through Alpha-Hemolysin (α-HL) and Mycobacterium smegmatis Porin A (MspA) Nanopores. Journal of The Electrochemical Society 2022, 169 (5), 057510. [PubMed: 35599744]

(21). Wanunu M; Morrison W; Rabin Y; Grosberg AY; Meller A Electrostatic focusing of unlabelled DNA into nanoscale pores using a salt gradient. Nature nanotechnology 2010, 5 (2), 160–165.

(22). Freedman KJ; Bastian AR; Chaiken I; Kim MJ Solid-state nanopore detection of protein complexes: applications in healthcare and protein kinetics. Small 2013, 9 (5), 750–759. [PubMed: 23074081]

(23). Sze JY; Ivanov AP; Cass AE; Edel JB Single molecule multiplexed nanopore protein screening in human serum using aptamer modified DNA carriers. Nature communications 2017, 8 (1), 1–10.

(24). Meier NR; Jacobsen M; Ottenhoff TH; Ritz N A systematic review on novel Mycobacterium tuberculosis antigens and their discriminatory potential for the diagnosis of latent and active tuberculosis. Frontiers in immunology 2018, 9, 2476. [PubMed: 30473692]

(25). Cardona P-J Understanding Tuberculosis: Deciphering the Secret Life of the Bacilli; IntechOpen, Rijeka, Croatia, 2012.

(26). Sreejit G; Ahmed A; Parveen N; Jha V; Valluri VL; Ghosh S; Mukhopadhyay S The ESAT-6 protein of Mycobacterium tuberculosis interacts with beta-2-microglobulin (β2M) affecting antigen presentation function of macrophage. PLoS pathogens 2014, 10 (10), e1004446. [PubMed: 25356553]

(27). Hill PC; Jackson-Sillah D; Fox A; Franken KL; Lugos MD; Jeffries DJ; Donkor SA; Hammond AS; Adegbola RA; Ottenhoff TH ESAT-6/CFP-10 fusion protein and peptides for optimal diagnosis of mycobacterium tuberculosis infection by ex vivo enzyme-linked immunospot assay in the Gambia. Journal of clinical microbiology 2005, 43 (5), 2070–2074. [PubMed: 15872224]

(28). Shen G-H; Chiou C-S; Hu S-T; Wu K-M; Chen J-H Rapid identification of the Mycobacterium tuberculosis complex by combining the ESAT-6/CFP-10 immunochromatographic assay and smear morphology. Journal of clinical microbiology 2011, 49 (3), 902–907. [PubMed: 21159936]

(29). Arend SM; van Meijgaarden KE; de Boer K; de Palou EC; van Soolingen D; Ottenhoff TH; van Dissel JT Tuberculin skin testing and in vitro T cell responses to ESAT-6 and culture filtrate protein 10 after infection with Mycobacterium marinum or M. kansasii. The Journal of infectious diseases 2002, 186 (12), 1797–1807. [PubMed: 12447766]

(30). van Ingen J; de Zwaan R; Dekhuijzen R; Boeree M; van Soolingen D Region of difference 1 in nontuberculous Mycobacterium species adds a phylogenetic and taxonomical character. Journal of bacteriology 2009, 191 (18), 5865–5867. [PubMed: 19617365]

(31). Liu C; Lyon CJ; Bu Y; Deng Z; Walters E; Li Y; Zhang L; Hesseling AC; Graviss EA; Hu Y Clinical evaluation of a blood assay to diagnose paucibacillary tuberculosis via bacterial antigens. Clinical chemistry 2018, 64 (5), 791–800. [PubMed: 29348166]

(32). Mao L; LaCourse SM; Kim S; Liu C; Ning B; Bao D; Fan J; Lyon CJ; Sun Z; Nachman S Evaluation of a serum-based antigen test for tuberculosis in HIV-exposed infants: a diagnostic accuracy study. BMC medicine 2021, 19 (1), 1–12. [PubMed: 33390155]

(33). He Y; Lyon CJ; Nguyen DT; Liu C; Sha W; Graviss EA; Hu TY Serum-based diagnosis of pediatric tuberculosis by assay of Mycobacterium tuberculosis factors: a retrospective cohort study. Journal of Clinical Microbiology 2021, 59 (2), 10.1128/jcm.01756-01720.

(34). Liu C; Zhao Z; Fan J; Lyon CJ; Wu H-J; Nedelkov D; Zelazny AM; Olivier KN; Cazares LH; Holland SM Quantification of circulating Mycobacterium tuberculosis antigen peptides allows rapid diagnosis of active disease and treatment monitoring. Proceedings of the National Academy of Sciences 2017, 114 (15), 3969–3974.

(35). World Health Organization. WHO operational handbook on tuberculosis: module 3: diagnosis: tests for tuberculosis infection. 2022. https://www.who.int/publications/i/item/9789240058347.

(36). Abualrihy A; Minasian D; Wolfson I; Oley W Tuberculosis Screening. In The Resident's Guide to Ambulatory Care, 7th ed.; Anadem Publishing, Columbus, Ohio, US, 2015; pp147–151.

(37). World Health Organization. Use of tuberculosis interferon-gamma release assays (IGRAs) in low-and middle-income countries: policy statement. 2011. https://www.who.int/publications/i/item/9789241502672.

(38). Sheka D; Alabi N; Gordon PM Oxford nanopore sequencing in clinical microbiology and infection diagnostics. Briefings in Bioinformatics 2021, 22 (5), 1–17. [PubMed: 33401308]

(39). Lu H; Giordano F; Ning Z Oxford Nanopore MinION sequencing and genome assembly. Genomics, proteomics & bioinformatics 2016, 14 (5), 265–279.

(40). Graham SM; Cuevas LE; Jean-Philippe P; Browning R; Casenghi M; Detjen AK; Gnanashanmugam D; Hesseling AC; Kampmann B; Mandalakas A Clinical case definitions for classification of intrathoracic tuberculosis in children: an update. Clinical Infectious Diseases 2015, 61 (suppl_3), S179–S187.

(41). Sze JY; Ivanov AP; Cass AE; Edel JB Single molecule multiplexed nanopore protein screening in human serum using aptamer modified DNA carriers. Nature communications 2017, 8 (1), 1552.

(42). Chuah K; Wu Y; Vivekchand S; Gaus K; Reece PJ; Micolich AP; Gooding JJ Nanopore blockade sensors for ultrasensitive detection of proteins in complex biological samples. Nature communications 2019, 10 (1), 2109.

(43). Wu Y; Chuah K; Gooding JJ Evaluating the sensing performance of nanopore blockade sensors: A case study of prostate-specific antigen assay. Biosensors and Bioelectronics 2020, 165, 112434. [PubMed: 32729547]

(44). Tang H; Wang H; Yang C; Zhao D; Qian Y; Li Y Nanopore-based strategy for selective detection of single carcinoembryonic antigen (CEA) molecules. Analytical chemistry 2020, 92 (4), 3042–3049. [PubMed: 31970978]

(45). Houghtaling J; List J; Mayer M Nanopore-Based, Rapid Characterization of Individual Amyloid Particles in Solution: Concepts, Challenges, and Prospects. Small 2018, 14 (46), 1802412.

(46). Zeng T; Liu L; Li T; Li Y; Gao J; Zhao Y; Wu H-C Detection of 5-methylcytosine and 5-hydroxymethylcytosine in DNA via host–guest interactions inside α-hemolysin nanopores. Chemical science 2015, 6 (10), 5628–5634. [PubMed: 28757950]

(47). Zhang Z; Li T; Sheng Y; Liu L; Wu HC Enhanced sensitivity in nanopore sensing of cancer biomarkers in human blood via click chemistry. Small 2019, 15 (2), 1804078.

(48). Wei X; Zhang Z; Wang X; Lenhart B; Gambarini R; Gray J; Liu C Insight into the effects of electrochemical factors on host-guest interaction induced signature events in a biological nanopore. Nanotechnology and Precision Engineering 2020, 3 (1), 2–8. [PubMed: 33786424]

(49). Wei X; Wang X; Zhang Z; Luo Y; Wang Z; Xiong W; Jain PK; Monnier JR; Wang H; Hu TY A click chemistry amplified nanopore assay for ultrasensitive quantification of HIV-1 p24 antigen in clinical samples. Nature Communications 2022, 13 (1), 6852.

(50). DiNardo AR; Detjen A; Ustero P; Ngo K; Bacha J; Mandalakas AM Culture is an imperfect and heterogeneous reference standard in pediatric tuberculosis. Tuberculosis 2016, 101, S105–S108.

(51). Gupta N; Kashyap B; Dewan P; Hyanki P; Singh N Clinical spectrum of pediatric tuberculosis: a microbiological correlation from a tertiary care center. Journal of Tropical Pediatrics 2019, 65 (2), 130–138. [PubMed: 29846733]

(52). Nhu NTQ; Ha DTM; Anh ND; Thu DDA; Duong TN; Quang ND; Lan NTN; Van Quyet T; Tuyen NTB; Ha VT Evaluation of Xpert MTB/RIF and MODS assay for the diagnosis of pediatric tuberculosis. BMC infectious diseases 2013, 13 (1), 1–9. [PubMed: 23280237]

(53). Chiappini E; Lo Vecchio A; Garazzino S; Marseglia G; Bernardi F; Castagnola E; Tomà P; Cirillo D; Russo C; Gabiano C Recommendations for the diagnosis of pediatric tuberculosis. European Journal of Clinical Microbiology & Infectious Diseases 2016, 35, 1–18. [PubMed: 26476550]

(54). santé O. m. d. l. Global tuberculosis report 2019; World health organization., 2019.

(55). Monkongdee P; McCarthy KD; Cain KP; Tasaneeyapan T; Dung NH; Lan NT; Yen NT; Teeratakulpisarn N; Udomsantisuk N; Heilig C Yield of acid-fast smear and mycobacterial culture for tuberculosis diagnosis in people with human immunodeficiency virus. American journal of respiratory and critical care medicine 2009, 180 (9), 903–908. [PubMed: 19628775]

(56). Organization, W. H. Systematic screening for active tuberculosis: principles and recommendations; World Health Organization, 2013.

(57). Dunlap NE; Bass J; Fujiwara P; Hopewell P; Horsburgh C; Salfinger M; Simone P Diagnostic standards and classification of tuberculosis in adults and children. American Journal of Respiratory and Critical Care Medicine 2000, 161 (4), 1376–1395. [PubMed: 10764337]

(58). Swaminathan S; Rekha B Pediatric tuberculosis: global overview and challenges. Clinical infectious diseases 2010, 50 (Supplement_3), S184–S194. [PubMed: 20397947]

(59). Cruz AT; Starke JR Clinical manifestations of tuberculosis in children. Paediatric respiratory reviews 2007, 8 (2), 107–117. [PubMed: 17574154]

(60). Eamranond P; Jaramillo E Tuberculosis in children: reassessing the need for improved diagnosis in global control strategies. The International Journal of Tuberculosis and Lung Disease 2001, 5 (7), 594–603. [PubMed: 11467365]

(61). Ioannidis P; Papaventsis D; Karabela S; Nikolaou S; Panagi M; Raftopoulou E; Konstantinidou E; Marinou I; Kanavaki S Cepheid GeneXpert MTB/RIF assay for Mycobacterium tuberculosis detection and rifampin resistance identification in patients with substantial clinical indications of tuberculosis and smear-negative microscopy results. Journal of clinical microbiology 2011, 49 (8), 3068–3070. [PubMed: 21677069]

(62). Evans CA GeneXpert—a game-changer for tuberculosis control? PLoS medicine 2011, 8 (7), e1001064. [PubMed: 21814497]

(63). Denkinger CM; Pai M; Patel M; Menzies D Gamma interferon release assay for monitoring of treatment response for active tuberculosis: an explosion in the spaghetti factory. Journal of clinical microbiology 2013, 51 (2), 607–610. [PubMed: 23175268]

(64). Department of Health and Human Servces, Centers for Disease Control and Prevention. Morbidity and Mortality Weekly Report. Updated guidelines for using interferon gamma release assays to detect Mycobacterium tuberculosis infection--United States, 2010. Vol. 59, June 25, 2010. https://stacks.cdc.gov/view/cdc/5670.

(65). Dodd PJ; Yuen CM; Sismanidis C; Seddon JA; Jenkins HE The global burden of tuberculosis mortality in children: a mathematical modelling study. The Lancet Global Health 2017, 5 (9), e898–e906. [PubMed: 28807188]

(66). Meher AK; Bal NC; Chary KV; Arora A Mycobacterium tuberculosis H37Rv ESAT-6–CFP-10 complex formation confers thermodynamic and biochemical stability. The FEBS journal 2006, 273 (7), 1445–1462. [PubMed: 16689931]

(67). Mor P; Dahiya B; Sharma S; Sheoran A; Parshad S; Malhotra P; Gulati P; Mehta PK Diagnosis of peritoneal tuberculosis by real-time immuno-PCR assay based on detection of a cocktail of Mycobacterium tuberculosis CFP-10 and HspX proteins. Expert Review of Gastroenterology & Hepatology 2022, 16 (6), 577–586. [PubMed: 35678762]

(68). Munk ME; Arend SM; Brock I; Ottenhoff TH; Andersen P Use of ESAT-6 and CFP-10 antigens for diagnosis of extrapulmonary tuberculosis. The Journal of Infectious Diseases 2001, 183 (1), 175–176. [PubMed: 11106545]

(69). Seifert M; Vargas E; Ruiz-Valdepeñas Montiel V; Wang J; Rodwell TC; Catanzaro A Detection and quantification of Mycobacterium tuberculosis antigen CFP10 in serum and urine for the rapid diagnosis of active tuberculosis disease. Scientific Reports 2021, 11 (1), 19193. [PubMed: 34584117]

(70). Bekmurzayeva A; Sypabekova M; Kanayeva D Tuberculosis diagnosis using immunodominant, secreted antigens of Mycobacterium tuberculosis. Tuberculosis 2013, 93 (4), 381–388. [PubMed: 23602700]

(71). Zhang C; Song X; Zhao Y; Zhang H; Zhao S; Mao F; Bai B; Wu S; Shi C Mycobacterium tuberculosis secreted proteins as potential biomarkers for the diagnosis of active tuberculosis and latent tuberculosis infection. Journal of clinical laboratory analysis 2015, 29 (5), 375–382. [PubMed: 25131423]

(72). Organization WH High priority target product profiles for new tuberculosis diagnostics: report of a consensus meeting, 28–29 April 2014, Geneva, Switzerland; World Health Organization, 2014.

(73). Marais BJ; Gie RP; Obihara CC; Hesseling A; Schaaf H; Beyers N Well defined symptoms are of value in the diagnosis of childhood pulmonary tuberculosis. Archives of disease in childhood 2005, 90 (11), 1162–1165. [PubMed: 16131501]

(74). Pfyffer GE; Wittwer F Incubation time of mycobacterial cultures: how long is long enough to issue a final negative report to the clinician? Journal of clinical microbiology 2012, 50 (12), 4188. [PubMed: 23052304]

(75). Ogwang S; Mubiri P; Bark CM; Joloba ML; Boom WH; Johnson JL Incubation time of Mycobacterium tuberculosis complex sputum cultures in BACTEC MGIT 960: 4 weeks of negative culture is enough for physicians to consider alternative diagnoses. Diagnostic microbiology and infectious disease 2015, 83 (2), 162–164. [PubMed: 26239846]

(76). Clouse K; Page-Shipp L; Dansey H; Moatlhodi B; Scott L; Bassett J; Stevens W; Sanne I Implementation of Xpert MTB/RIF for routine point-of-care diagnosis of tuberculosis at the primary care level. South African Medical Journal 2012, 102 (10), 805–807. [PubMed: 23034211]

(77). van Zyl-Smit RN; Binder A; Meldau R; Mishra H; Semple PL; Theron G; Peter J; Whitelaw A; Sharma SK; Warren R Comparison of quantitative techniques including Xpert MTB/RIF to evaluate mycobacterial burden. PloS one 2011, 6 (12), e28815. [PubMed: 22216117]

(78). Walters E; van der Zalm MM; Demers A-M; Whitelaw A; Palmer M; Bosch C; Draper HR; Schaaf HS; Goussard P; Lombard CJ Specimen pooling as a diagnostic strategy for microbiologic confirmation in children with intrathoracic tuberculosis. The Pediatric infectious disease journal 2019, 38 (6), e128. [PubMed: 30418355]

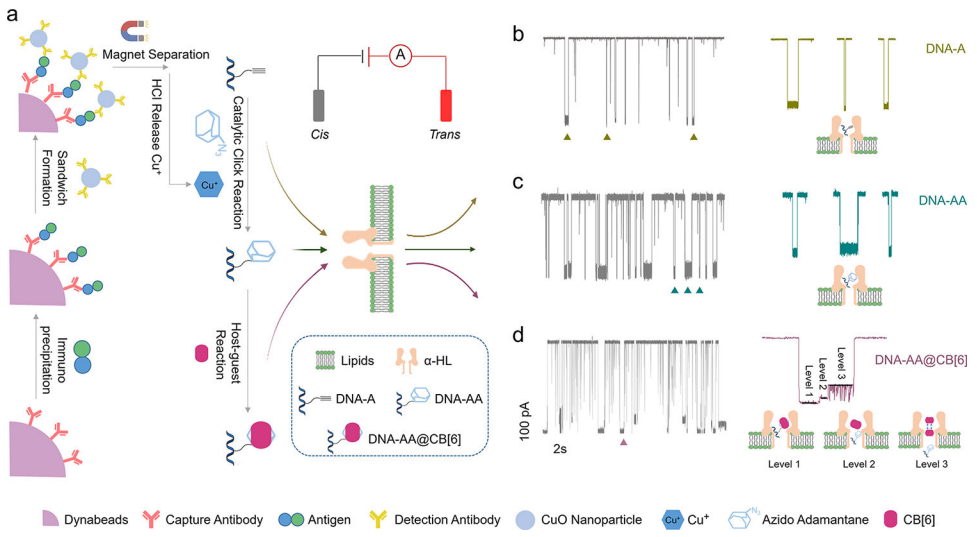

Figure 1.

Schematic illustration of the nanopore assay for ESAT-6/CFP-10 antigen complex quantification. **a**: Capture antibody-modified dynabeads immunoprecipitate ESAT-6/CFP-10 antigen complex from serum samples, followed by specific binding of detection antibody-modified CuO nanoparticles to form a sandwich structure. Sandwich structures were then magnetically separated and Cu^{+} was released by hydrochloric acid to catalyze the click reaction between DNA-alkyne (DNA-A) and azido adamantane (AA) to form DNA-AA with amplification. Finally, DNA-AA@CB[6] probes were formed via host-guest interaction with CB[6]. **b**: Translocation recordings of DNA-A through a single α-HL nanopore and the corresponding nanopore steric hindrance status. **c**: Translocation recordings of DNA-AA through a single α-HL nanopore and the corresponding nanopore steric hindrance status. **d**: Translocation recordings of DNA-AA@CB[6] through a single α-HL nanopore. Three blockade levels of the characteristic signal indicate the molecular status inside the nanopore: DNA translocation, CB[6] dissociation, and CB[6] oscillation, respectively. Data was acquired using 3 M KCl, 10 mM Tris buffer at pH 8.0 and under a 160 mV *trans* potential unless otherwise stated.

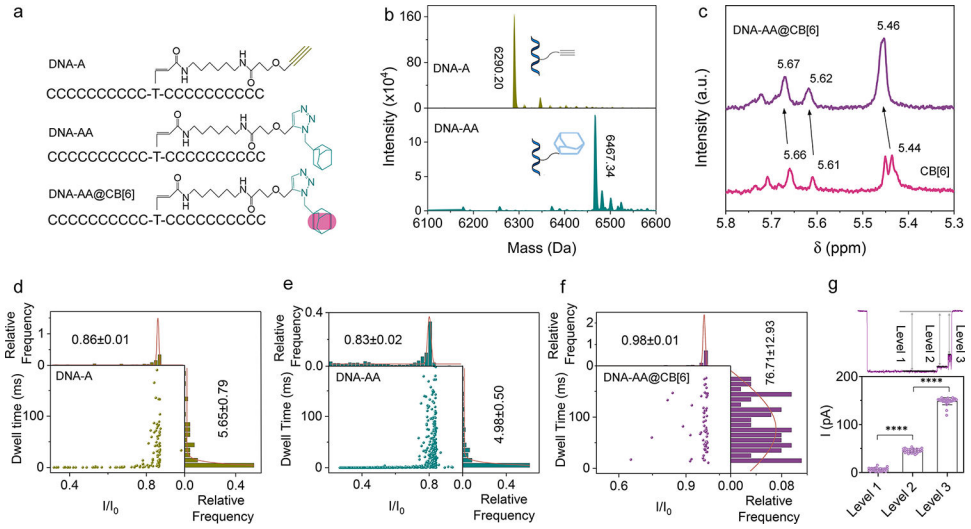

Figure 2.

Characterization of DNA complexes and their translocation signals. **a**: Chemical structure of DNA-A, DNA-AA, and DNA-AA@CB[6]. DNA (5′-CCCCCCCCCCTCCCCCCCCCC) modified with an alkyne moiety on the T base formed DNA-A; a click reaction between the alkyne moiety and azide adamantane formed DNA-AA; non-covalent host-guest interaction between DNA-AA and CB[6] formed a DNA-AA@CB[6] probe. **b**: Electrospray ionization mass spectrograms of reactant DNA-A and product DNA-AA of the click reaction. **c**: ^{1}H NMR (300 MHz) spectra of reactant CB[6] and achieved DNA-AA@CB[6] probes. The host-guest interaction can be confirmed by the chemical shift of protons of the CB[6] molecule from methylene (CH_2) groups (5.66 ppm and 5.44 ppm) and tertiary C-H groups (5.61 ppm). **d-f**: Blockade vs. dwell time translocation profiles of (d) DNA-A, (e) DNA-AA, and (f) DNA-AA@CB[6]. Top: histograms of relative frequency of I/I_0 with Gaussian fitting. Right: histograms of relative frequency of dwell time with exponential fitting. **g**: A typical characteristic oscillation signal generated by the DNA-AA@CB[6] probe translocating an α-HL nanopore. The signal is characterized by a pattern with 3 levels. Average currents of Level 1, 2, and 3 in oscillation signals were analyzed by one-way ANOVA. **** indicates P<0.001 Level 1 *vs.* Level 2, Level 2 *vs.* Level 3 by multiple comparisons, N=30). Data was acquired using 3 M KCl, 10 mM Tris buffer at pH 8.0 and under a 160 mV trans potential unless otherwise stated.

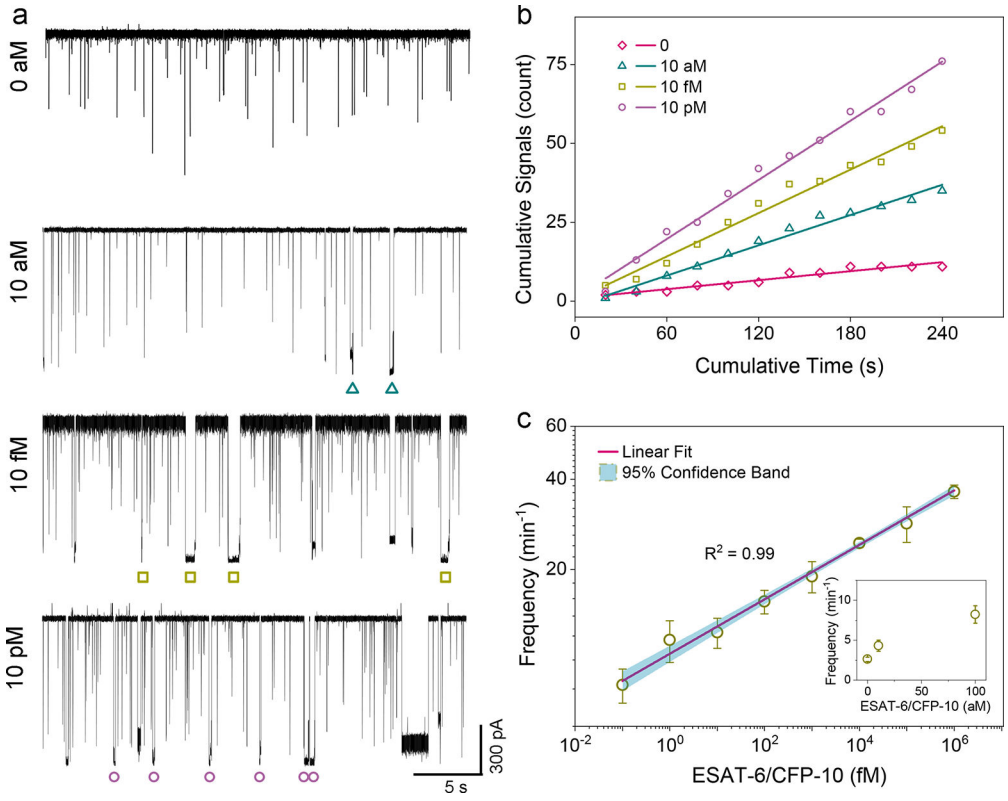

Figure 3.

Quantification of ESAT-6/CFP-10 in human serum. **a**: Raw translocation recordings of serially diluted ESAT-6/CFP-10 antigens (0 aM, 10 aM, 10 fM, and 10 pM) through single α-HL nanopores; triangles, squares, and circles indicate oscillation signals in different data sets. **b**: Capture rate of oscillation signals in different ESAT-6/CFP-10 antigen concentrations. The cumulative numbers of signals were counted every 20s. Solid lines indicate linear regression. **c**: Correlations between oscillation signal frequency and ESAT-6/CFP-10 antigen concentration in human serum within the range of 0.1–10^6 fM. Inset shows the correlations within attomolar range (0, 10 and 100 aM). Data represents mean ± SD of three replicates. Solid line indicates linear regression. Shadow indicates limits of 95% confidence interval. Data was acquired using 3 M KCl, 10 mM Tris buffer at pH 8.0 and under a 160 mV *trans* potential unless otherwise specified.

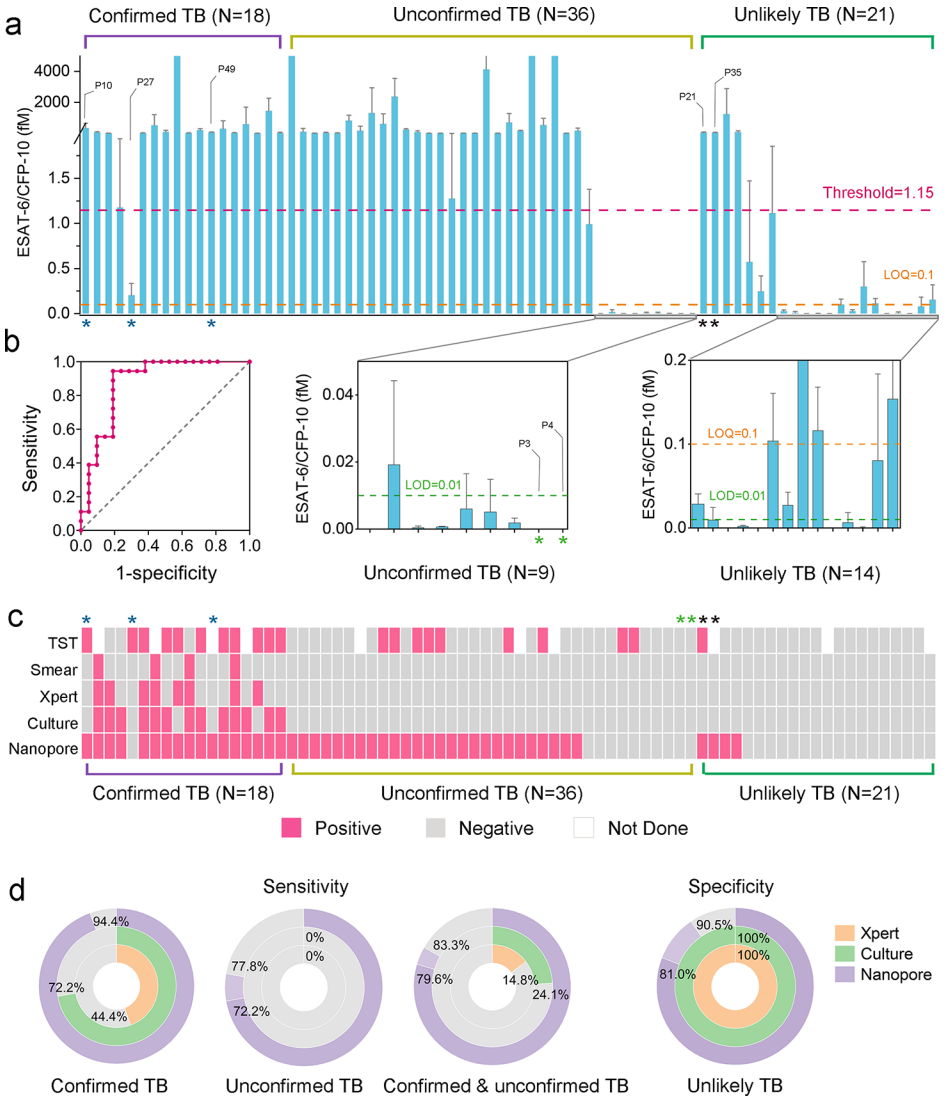

Figure 4.

Clinical validation in a pilot pediatric cohort. Study participants numbered P1 to P75 were classified into three groups according to NIH definitions: confirmed TB (N=18), unconfirmed TB (N=36), and unlikely TB (N=21). **a:** Quantification of ESAT-6/CFP-10 antigen complex in different groups by the nanopore assay. Insets show cases with low concentration ESAT-6/CFP-10. The green line indicates LOD (0.01 fM); the yellow line indicates LOQ (0.10 fM); the red line indicates the optimal threshold (1.15 fM) from the receiver operating characteristic (ROC) curve. Data represents mean ± SD of three replicates. Data was acquired using 3 M KCl, 10 mM Tris buffer at pH 8.0 and under a 160 mV *trans* potential unless otherwise stated. **b**: ROC curve of the 75 clinical samples. Area under the ROC curve is 0.8757, P<0.0001, threshold is 1.15 fM, sensitivity is 94.44%, specificity is 80.95%. **c:** Cluster map of clinical test results and nanopore test results for all participants. Clinical tests include TST, smear, Xpert, *Mtb* culture. Nanopore results are called based on the threshold. Blue stars indicate cases confirmed at follow up; green stars indicate cases redesignated to unlikely TB; and black stars indicate cases redesignated to

unconfirmed TB upon further review of treatment and follow up information. **d:** Sensitivity and specificity comparison among nanopore, Xpert, and *Mtb* culture tests, including updated sensitivities and specificities after reclassification (refer to Discussion).

Table 1.

Demographics and clinical characteristics of the pilot cohort.

Characteristic	Confirmed TB[γ]	Unconfirmed TB[ϕ]	Unlikely TB[†]	All Participants
Demographics				
Male sex no./total no. (%)	8/18 (44.44)	21/36 (58.33)	15/21 (71.43)	44/75 (58.67)
Median Age (range) yr	2 (0.58–8)	2 (0.83–12)	3 (0.25–10)	2 (0.25–12)
Clinical Characteristics (%)				
Positive Xpert	8/18 (44.44)	0/36 (0)	0/21 (0)	8/75 (10.67)
Negative Xpert	10/18 (55.56)	36/36 (100)	21/21 (100)	67/75 (89.33)
Positive *Mtb* Culture	13/18 (72.22)	0/36(0)	0/21 (0)	13/75 (17.33}
Negative *Mtb* Culture	5/18 (27.78)	36/36 (100)	21/21 (100)	62/75 (82.67)
Positive Tuberculin Skin Test[*]	11/18 (61.11)	9/36 (25.00)	1/21 (4.76)	21/75 (28.00)
Negative Tuberculin Skin Test	3/18 (16.67)	24/36 (66.67)	17/21 (80.95)	44/75 (58.67)
Significant TB Exposure[#]	8/18 (44.44)	14/36 (38.89)	3/21 (14.29)	25/75 (33.33)
Well Defined Symptoms[+]	15/18 (83.33)	33/36 (91.67)	17/21 (80.95)	65/75 (86.67)
TB Consistent Chest Radiograph	12/18 (66.67)	12/36 (33.33)	2/21 (9.52)	26/75 (34.67)
Positive Response to TB Treatment	15/18 (83.33)	22/36 (61.11)	0/21 (0)	37/75 (49.33)
Nanopore Result (%)				
Above LOQ	18/18 (100)	27/36 (75.00)	11/21 (52.38)	56/75 (74.67)
Above Threshold	17/18 (94.44)	26/36 (72.22)	4/21 (19.05)	47/75 (62.67)

[γ] Confirmed TB cases (positive *Mtb* culture or positive Xpert results for respiratory or stool samples).

[ϕ] Unconfirmed TB cases (if positive for ≥2 of the following criteria: significant TB exposure, positive tuberculin skin test, TB-associated symptoms, and abnormal TB-consistent chest radiograph.

[†] Unlikely TB (if lacked two criteria for unconfirmed TB).

[*] Positive tuberculin skin test (the person's body was infected with TB bacteria).

[#] Significant TB exposure (index case=mother or household member, or someone spending >= 4 hours a day with child).

[+] Well defined symptoms of pediatric TB disease (2005).

Table 2.

Discrepancy between nanopore results and clinical classification.

	Patient No.	ESAT-6/ CFP-10 (fM)	Well Defined Symptoms[+]	TB Contact	TST	Chest X-ray	Treatment Status[*]	Treatment Response	Previous TB
Unconfirmed TB	P3	0.00	Y	N	Neg.	TB	Symptomatic control Not treated	Followed up and did not improve[#]	Y
	P4	0.00	Y	N	Neg.	TB	Symptomatic control Not treated	Followed up and did not improve[#]	N
Unlikely TB	P21	50.59	Y	N	Not done	NotTB	Control to case T reated	Not followed up	N
	P35	49.60	Y	N	Pos.	NotTB	Symptomatic control Not treated (Isoniazid preventive therapy)	Followed up and improved	N

[+]Well defined symptoms of pediatric TB disease (2005).

[*]Treatment status (symptomatic control: children were never treated for active TB: control to case: children started TB treatment later > 2 months after baseline).

[#]Refer to the discussion for more details.